LA-UR-84-1391

LA-UR--84-1391

DE84 011353

Los Alamos National Laboratory is operated by the University of California for the United States Department of Energy under contract W-7405-ENG-36.

CONF-840256--2

TITLE: ION REFLECTION, GYRATION, AND DISSIPATION AT SUPERCRITICAL SHOCKS

AUTHOR(S): J.T. Gosling and A.E. Robson

SUBMITTED TO: Proceedings of the Napa Shock Conference held in Napa Valley, CA, 20-24 February 1984

## DISCLAIMER







Los Alamos Los Alamos National Laboratory
Los Alamos, New Mexico 87545

# ION REFLECTION, GYRATION, AND DISSIPATION AT SUPERCRITICAL SHOCKS

J. T. Gosling
University of California
Los Alamos National Laboratory
Los Alamos, NM 87545

A. E. Robson
Naval Research Laboratory
Washington, DC 20375

## 1. Introduction

Characteristic changes occur in collisionless shock structure as the Mach number of the upstream flow is increased above a critical value. A magnetic foot develops upstream of the main shock ramp, and an overshoot appears at the top of the ramp. These changes in a shock's magnetic profile are closely associated with the reflection at the shock of a fraction of the incoming ions. Such reflection plays an important role in ion dissipation at high Mach number shocks. The critical Alfvén Mach number, $M_c$, where ion reflection occurs depends upon upstream conditions, but typically $M_c \approx 2-3$. A shock whose Alfvén Mach number exceeds $M_c$ is known as a supercritical shock.

The reflection of incident ions is caused by a combination of electrostatic and magnetic forces and is nearly specular in nature. The initial trajectory of a specularly reflected ion depends crucially on $\theta_{Bn}$, the angle between the upstream magnetic field, $\underline{B}$, and the local shock normal, $\hat{n}$. For $\theta_{Bn} > 45^\circ$ (quasi-perpendicular shock) specularly reflected ions have guiding center motions which are directed downstream. Reflected ions in this geometry thus return to the shock and gyrate downstream where they contribute importantly to downstream thermalization. However, for $\theta_{Bn} < 45^\circ$ (quasi-parallel shock) specularly reflected ions gyrate upstream when the upstream magnetic field is steady. Thus under steady upstream conditions, specularly reflected ions cannot contribute directly to downstream thermalization in the quasi-parallel geometry. This fact may be of fundamental importance in explaining observed differences between quasi-parallel and quasi-perpendicular shock structure.

The purpose of the present paper is to review laboratory and space measurements pertaining to initial ion reflection and subsequent gyration at supercritical shocks. We will be concerned with providing a simple conceptual

framework with which such reflection and gyration and its role in producing dissipation at the shock can be understood. Details of the actual reflection mechanism and the relative importance of electrostatic forces and magnetic forces in producing ion reflection have been addressed in considerable depth in recent simulation studies (e.g., Leroy et al., 1981, 1982) and are reviewed elsewhere in this volume by Goodrich (1984). Multiple reflections and the production of a variety of upstream suprathermal ion populations by reflections and other mechanisms likewise are treated elsewhere in this volume by Thomsen (1984).

## 2. Laboratory Results

Early space measurements were sufficient to establish the existence of collisionless shocks in the solar wind (e.g., Sonett et al., 1964, Ness et al., 1964) and to study certain macroscopic aspects of shocks such as their deceleration during outward transit from the sun (e.g., Gosling et al., 1968) and the shape of the earth's bow shock (e.g., Holzer et al., 1966). However, the measurements (particularly of the plasma) were inadequate to resolve the structure of the shock layer or to study dissipation processes at the shock. Such studies became possible in the early 70's with the launching of improved plasma instruments aboard later satellites in the Vela, Imp, and Ogo series.

Only relatively recently, however, with the launch of the ISEE-1 and -2 satellites have high quality measurements of plasma distributions become available. Thus much of the early probing of collisionless shock structure was concentrated in laboratory experiments, whose prime impetus was derived from programs to harness nuclear fusion. Funding for such experiments was curtailed in the mid 70's.

Laboratory experiments of shocks were done almost exclusively using θ-pinch and Z-pinch devices and were conducted by a variety of groups around the world. These experiments provided controlled conditions (in contrast to space measurements) which could be repeated. Measurements were made of the magnetic field, $\underline{B}$, the electric potential, $\phi$, the electron density, $n_e$, electron temperature, $T_e$, and bulk flow velocity, V, as functions of position. In the larger experiments, such as those conducted at the University of Texas in Austin or at Culham Laboratories in England, the shocks were well separated (by several ion gyroradii) from the magnetic pistons driving them. Further, in these larger experiments the shocks were stationary long enough to permit i complete ion gyro-orbit downstream. On the other hand, the laboratory experiments, although collisionless downstream, were not unequivocally collisionless in the upstream region. Nevertheless, collisionless mechanisms were necessary to account for the structure of the observed shocks.

One drawback of the laboratory experiments was that they did not provide information on the shapes of distribution functions. Nor did they, for the most part, provide measurements of ions. Most experiments were done in the nearly perpendicular geometry ($\theta_{Bn} \approx 90^\circ$), although oblique geometries were utilized in some experiments. Paul (1969) and Robson (1969) have provided excellent reviews of the early laboratory experiments done in the nearly perpendicular geometry and in the oblique geometry respectively. Here we provide an extremely limited review of those laboratory results that bear directly on the problem of ion reflection and dissipation at supercritical shocks.

In most experiments it was found that as the Mach number of the upstream flow was increased, characteristic changes occurred in shock structure. Figure 1, which shows magnetic field and electric potential measurements

through two different Mach number shocks, illustrates these changes. When the upstream Mach number is low (upper panel), both the magnetic field and the electric potential rise sharply through the shock on a scale size which is determined by a competition between resistive and dispersive effects (e.g., Mellott and Greenstadt, 1984). However, as the upstream Mach number increases (lower panel), a long foot develops upstream of the main shock ramp when the shock geometry is nearly perpendicular. (For some reason the foot was not observed in oblique geometries.) Following the suggestion (e.g., Woods, 1969) that the foot was caused by reflected, gyrating ions, experiments were conducted to detect such ions directly in the nearly perpendicular geometry (Phillips and Robson, 1972).

Figure 2 illustrates the trajectory of a specularly reflected ion (i.e., an ion whose normal component of velocity is reversed at the shock) for arbitrary angle of incidence in the perpendicular geometry ($\theta_{Bn} = 90^{\circ}$). The reflected ion undergoes a partial gyration about $\underline{B}$ and then re-encounters the shock. Because the ion gains energy from the interplanetary $\underline{V} \times \underline{B}$ electric field during the first half of its gyro-orbit, it has sufficient energy upon reentry into the shock to penetrate into the downstream region. With a coordinate system fixed in the shock as shown in the figure, the orbit of the reflected ion in the upstream region is described by

$$x = \frac{V\cos\theta_{vn}}{\Omega_p} \left[2 \sin \Omega_p t - \Omega_p t\right] \tag{1}$$

$$y = -\frac{2V\cos\theta_{vn}}{\Omega_p} \left[\cos\Omega_p t - 1\right] - Vt\sin\theta_{vn} \tag{2}$$

where $\Omega_p = \frac{qB}{m_p c}$, V is the incident flow speed, $\theta_{vn}$ is the acute angle between $\underline{V}$

and $\Omega_i$ and t is the time since reflection. The turn-around point occurs at $0.685\ R_{gi}\cos\theta_{vn}$ upstream, at which point the ion is moving parallel to the shock with a speed $\frac{1}{2}V\cos\theta_{vn}\ (\sqrt{3} + \tan\theta_{vn})$. Here $R_{gi} = \frac{V}{\Omega_{pi}}$. Measured foot lengths are comparable to $0.685\ R_{gi}\cos\theta_{vn}$.

Phillips and Robson's measurements of electric potential jump at the shock (normalized to the incident ion flow energy) and reflected ion current as functions of Alfvén Mach number, $M_A$, for $\theta_{vn} = 0^\circ$, $\theta_{Bn} = 90^\circ$ are shown in the top and bottom panels respectively of Figure 3. No reflected ions were detected at $M_A < 3$, but above that value the reflected ion current increased nearly linearly with increasing $M_A$. The onset of ion reflection was simultaneous with the development of an upstream foot in the field and potential profiles, and the reflected ions were spatially coincident with the foot. Importantly, the normalized potential jump across the shock decreased with the onset of ion reflection and was less than 1.0. This indicated that ion reflection was not caused by the potential jump acting alone. It was suggested that the ions might have been reflected from peaks in an (undetected) oscillatory wave train behind the shock, or that a subshock within the shock ramp might sufficiently heat the incoming ions that some of them might not be able to overcome the potential jump. However, space measurements (e.g., Neugebauer, 1970; Montgomery et al., 1970; Bame et al., 1979; Paschmann et al., 1982) indicate that the ions are not significantly heated in the shock ramp, and it now appears that magnetic forces associated with the reflected, gyrating ions themselves sufficiently augment the electric forces acting on the incident ions to cause further reflection (Leroy et al., 1981, 1982).

The laboratory measurements thus established unequivocally that characteristic changes in nearly perpendicular shock profiles occurred at an Alfvén Mach number of ~3. These changes in shock structure were intimately

associated with the onset of ion reflection at the shock. Hydromagnetic theory predicts the existence of a critical Mach number, $M_c$, above which additional dissipation must occur at the shock (Woods, 1969; Coronitti, 1970). This critical Mach number occurs when the downstream flow speed normal to the shock becomes subsonic. For usual laboratory conditions $M_c \approx 2.8$. As the dispersion in velocity space resulting from ion reflection represents a significant amount of dissipation, it appears that ion reflection is a shock's chosen way of achieving additional dissipation at a supercritical shock. It is not presently clear why ion reflection, rather than some other dissipation process, is the mode by which additional dissipation is achieved. Perhaps it is the only mode available.

## 3. Space Results

Most of our detailed information about ion reflection and dissipation at supercritical shocks in space plasmas is derived from studies of the Earth's bow shock. As the $M_A$ for the solar wind flow exceeds 4.4 about 95% of the time (Feldman et al., 1977), the bow shock on the sunward side of the Earth is usually supercritical. By way of contrast, most interplanetary shocks associated with solar activity or high speed stream steepening are subcritical at 1AU. Another difficulty with studies of interplanetary shocks is that they pass over a spacecraft too quickly for shock structure to be resolved well even with the best of the present generation of space plasma experiments.

When the first detailed measurements were made near the Earth's bow shock, it was discovered that secondary peaks appeared in ion spectra obtained immediately upstream and downstream of the shock (Montgomery et al., 1970; Formisano and Hedgecock, 1973). It was surmised that these secondary peaks were associated with ion reflection at the shock and contributed importantly to

downstream ion thermalization. However, these early measurements lacked the temporal and angular resolution necessary to study the problem in depth. Such studies have become possible using measurements made with the fast plasma experiments on ISEE-1 and -2, which provide 2-dimensional snapshots of ion distribution functions in one spacecraft spin of 3 sec (Bame et al., 1978).

The schematic phase space plots in the lower portion of Figure 2 illustrate the positions in velocity space where specularly reflected ions would be observed at different distances from a perpendicular shock with arbitrary angle of incidence. It is assumed that the reflected ion orbits are unimpeded by collective interactions. (The laboratory measurements indicated little or no collective interactions in the foot regio.. (Phillips and Robson, 1972).) In the plasma rest frame the reflected ions initially have a speed $2\ V\cos\theta_{vn}$. Because an ion's kinetic energy is conserved in the plasma rest frame, the reflected ions' subsequent trajectory in velocity space is on a circle of radius $2\ V\cos\theta_{vn}$ in the plasma rest frame. As a spacecraft approaches the shock from the upstream side, reflected ions should first be observed moving parallel to the shock surface when the spacecraft enters the foot. The small open circle in the lower left-hand panel of Figure 2 indicates where the reflected ions would appear in velocity space. At the shock ramp, reflected ions should appear at two positions in velocity space (middle panel). The leftmost circle corresponds to ions just recently reflected, while the other small circle corresponds to ions returning to the shock, having been reflected earlier at a different shock position. Finally downstream (right-hand panel), reflected gyrating ions from various positions along the shock are observed simultaneously at a variety of phases in their gyro-orbits.

Figure 4 shows two ion velocity distributions obtained on the upstream side of an ISEE crossing of the bow shock on November 7, 1977. The panels shown are a small part of much larger sequences for this shock crossing published previously (Paschmann et al., 1982; Sckopke et al., 1983). Upstream conditions included a high Mach number ($M_A$ = 8.6), a high total plasma $\beta$ (3.9), and a nearly perpendicular geometry ($\theta_{Bn}$ = 85°). The velocity distributions are presented as contours of equal phase space density, f, in 2-dimensional velocity space oriented parallel to the ecliptic. The densely packed set of contours to the right of the + symbol in each panel is the incident solar wind beam, while the more widely spaced contours are reflected ions. These secondary ions first appear at the time shown in the left-hand panel when the satellite enters the foot of the shock. A more complicated arrangement of secondary ions is present in the snapshot taken at the shock ramp and shown in the right-hand panel. Comparison of the positions of the secondary ions in both panels with the schematic velocity space plots of Figure 2 indicates that the ions are the result of nearly specular reflection at the shock. However, it is apparent that the thermal spread of the secondary ions is greater than that of the incident solar wind. Sckopke et al. (1983) have shown that this probably indicates that a small fraction of the secondary ions are reflected in a nonspecular fashion at the shock.

Figure 5 illustrates a similar sequence of measured ion velocity distributions with emphasis on the downstream region for a crossing of the nearly perpendicular bow shock when $M_A$ was relatively low. As the shock speed past the spacecraft (~100 km $s^{-1}$) was relatively high on this occasion, the reflected ions were not resolved upstream of the shock. However, immediately downstream multiple peaks of secondary ions are observed lying approximately on a circle of radius 2 $V\cos\theta_{vn}$, as expected if the secondary ions are produced by

nearly specular reflection at the shock. The individual bunches of secondary ions do not maintain their identities for long. Frame 4 shows considerably less structure than Frame 2, and by Frame 6 the secondary ions are dispersed more or less uniformly around the 2 $V\cos\theta_{vn}$ circle. (Breaks in the contours occur at low speeds in the spacecraft frame where the count rate approaches instrument background.) Such dispersion in velocity space of the secondary ion bunches probably is a consequence of either kinematical phase mixing (e.g., Gurgiolo et al., 1983; Burgess and Schwartz, 1984) or ion beam instabilities (see Winske, 1984, this volume), and in this example occurs on a spatial scale of $\sim 12\ R_{gi}$ (Sckopke et al., 1983).

Downstream ion bunches such as those evident in Figure 5 are most clearly recognized at low Mach number crossings of the bow shock. At higher Mach numbers, the secondary ion bunches have higher relative densities and do not retain their individual identities for as long. In either case, as in the example shown above, the final downstream distribution generally consists of a directly transmitted beam of ions which is slowed and deflected at the shock but not strongly thermalized, plus a high energy shell of secondary ions. Such distributions are not Maxwellians. Figure 6 shows a series of cuts through the distributions measured downstream of the shock shown in Figure 4. The cuts were made parallel to the bulk flow direction and begin a few seconds after the shock crossing. Immediately downstream from the shock the reflected, gyrating ions are visible as a secondary peak in the spectra. Further downstream the secondary ions produce a broad shoulder at high energies which can persist all the way across the magnetosheath. (This shoulder should not be confused with "diffuse" ions which are often observed downstream of the shock, but at higher energies (Asbridge et al., 1978).) The dashed curve after the gap in the

sequence is a Maxwellian fit to the low energy core of the distribution, helping to emphasize the non-Maxwellian nature of the higher energy ions.

It has long been recognized that the coarse dispersion in velocity space resulting from ion reflection at a supercritical shock represents a substantial amount of dissipation, the magnitude of which depends upon the number of ions reflected. One can show (Sckopke et al., 1983) that the effective ion temperature in the foot of the shock, $T_f$, is given by

$$T_f = \eta_i T_i + \eta_r T_r + \eta_i \eta_r \left(\frac{m_p}{3k}\right)(\Delta V)^2 \qquad (3)$$

where k is Boltzmann's constant, $m_p$ is the proton mass, the subscripts i and r refer to the incident and reflected ions respectively, $|\underline{\Delta V}| \equiv |\underline{V}_r - \underline{V}_i| = 2\ V_i \cos\theta_{Vn}$, and $\eta_i \equiv \frac{n_i}{n_i+n_r}$ and $\eta_r = \frac{n_r}{n_i+n_r}$, n being the density. Because the ion distributions in the foot of the shock are highly nonthermal, $T_f$ is not a true temperature. Nevertheless, $T_f$ does provide an accurate measure of the internal energy present in the foot of the shock. Typically the intrinsic temperatures of the incident and reflected ions are $\sim 10^5$K, and for $\eta_r$ as low as 0.05, $T_f$ is dominated by the third term in (3). For typical solar wind speeds and $\eta_r = 0.10$, $T_f \gtrsim 10^6$ K, comparable to ion temperatures measured downstream of supercritical shocks. Thus, a large fraction of the ion heating achieved by a quasi-perpendicular, supercritical shock is associated ultimately with reflected ions which gyrate into the downstream region.

As the Mach number of a shock is increased, it is necessary for the shock to reflect increasingly larger fractions of the incident ions to produce the necessary downstream thermalization (see, for example, the lower panel in Figure 3). The amount of thermalization which must occur is related to the upstream conditions through the Rankine-Hugoniot relations and is thus not

arbitrary. We therefore expect that the fraction of ions reflected at a supercritical shock should be predictable from measurements of the upstream flow. A complication arises due to the fact that the Rankine-Hugoniot relations determine the combined change in electron and ion temperatures at the shock but do not specify how these changes must be subdivided between the two species (e.g., Sanderson and Uhrig, 1978). Measurements indicate that the electrons typically heat by a factor of ~2.5 at the shock, relatively independent of shock strength (e.g., Bame et al., 1979). This fact can be used to derive an expression for the downstream ion temperature in terms of upstream parameters. Equation 3 then allows one to estimate the fraction of ions reflected at the shock.

The result of applying the foregoing prescription for two different upstream plasma temperatures ($\beta$ = 0.1 and 10 respectively) is shown in Figure 7, where the predicted reflected fraction ($n_r/n_i$) is plotted versus magnetosonic Mach number, $M_{ms}$ (Paschmann and Sckopke, 1983). These calculations suggest that the reflected fraction should not exceed ~22% for typical solar wind conditions; otherwise the downstream temperature becomes too large to be consistent with the Rankine-Hugoniot relations. The model predictions appear to be in reasonable agreement with actual space observations (the two filled-in symbols) and with the results of recent computer simulations of the perpendicular bow shock by Leroy et al. (1982) (the asterisks).

Thus far we have assumed that ion reflection at the shock is nearly specular in nature. This assumption is in reasonable accord with both laboratory and space measurements already discussed and with simulation results (e.g., Quest et al., 1983; Leroy and Mauske, 1983). Specular reflection results because ions are essentially unmagnetized in their interaction with the shock (e.g., Schwartz et al., 1983; Thomsen et al., 1983). To see this, recall

that typical shock thicknesses, $\Delta L$, are of the order of $c/w_{pi} \approx 100$ km, where $w_{pi}$ is the ion plasma frequency (Russell and Greenstadt, 1979). The time for a solar wind parcel to transit the shock, $\tau_t$, is $\Delta L/V_i$, which for a solar wind speed of 400 km $s^{-1}$ is 0.25 s. A thermal ion gyroperiod, $T_g$, is $\frac{2\pi m_p c}{eB}$, which for a field of 5 nT is ~13 s. Thus, a thermal ion experiences only about 2% of its gyro-orbit as it transits the shock, and so is essentially unmagnetized during the encounter.

Although a specularly reflected ion is initially returned to the upstream region, its subsequent trajectory depends upon $\theta_{Bn}$ (Gosling et al., 1982). We have seen that in the perpendicular geometry ($\theta_{Bn} \approx 90^\circ$) specularly reflected ions gyrate downstream independent of $\theta_{vn}$. A simple geometrical construction can be used to examine the trajectories of specularly reflected ions for other field orientations. The construction to be described is planar in nature, but the result is perfectly general even when the vectors are not coplanar.

The left panel of Figure 8 shows vectors representing an incident ion velocity, $\underline{V}_i$, and the initial reflected velocity, $\underline{V}_r$, for an arbitrarily chosen $\theta_{vn}$ and assuming specular reflection at the shock. In the middle panels the perpendicular component of $\underline{V}_i$, $\underline{V}_\perp$, is drawn for $\theta_{Bn}$ values of 60° and 10°, respectively. The initial motion of the reflected ion leaving the shock can be decomposed into its guiding center motion, $\underline{V}_{gc}$, plus its gyrational motion $\underline{V}_g$. The guiding center motion, in turn, is the vector sum of the $\underline{E} \times \underline{B}$ drift perpendicular to $\underline{B}$, $\underline{V}_\perp$, and the motion parallel to $\underline{B}$. In the right panels of the figure we show the decomposition of $\underline{V}_r$ for $\theta_{Bn}$ values of 60° and 10°.

This construction illustrates two fundamental features of the trajectories of specularly reflected ions. First, one obtains greater gyrational motion in perpendicular geometries ($\theta_{Bn} > 45^\circ$) than in parallel geometries ($\theta_{Bn} < 45^\circ$). Second, the guiding center motion of a specularly reflected ion is initially

directed downstream for all $\theta_{Bn} > 45^{\circ}$ but is directed upstream for all $\theta_{Bn} < 45^{\circ}$. One can easily show in general that

$$|\underline{V}_g| = |2\ V_i\ \cos\theta_{vn}\ \sin\theta_{Bn}| \tag{4}$$

and

$$\underline{V}_{gc} \cdot \hat{n} = \underline{V}_i \cdot \hat{n}[1 - 2(\hat{n} \cdot \hat{B})^2] \tag{5}$$

where $\hat{B}$ is the unit vector along $\underline{B}$ chosen such that $\hat{B} \cdot \hat{n} < 90^{\circ}$.

The above construction shows that in the absence of interactions in the upstream region a specularly reflected ion must return to the shock for $\theta_{Bn} > 45^{\circ}$. In fact, for a limited range of $\theta_{Bn}$ values slightly less than $45^{\circ}$, a specularly reflected ion's gyrational motion causes it to re-encounter the shock even though the guiding center motion is directed upstream. Figure 9, from Schwartz et al. (1983), shows the result of a calculation of the returning ion's velocity perpendicular to the shock at re-encounter normalized to the perpendicular component of the initial incident velocity. Also shown is the gyrophase ($\Omega t^*$) at the time of re-encounter. For $\theta_{Bn} < 39.9^{\circ}$ specularly reflected ions gyrate upstream and do not re-encounter the shock. For $39.9^{\circ} < \theta_{Bn} < 45^{\circ}$ the reflected ion's gyrational motion returns it to the shock, but it arrives there with a speed perpendicular to the shock which is less than it had at its initial encounter. Such an ion probably undergoes further reflection at the shock. Finally, for $\theta_{Bn} > 45^{\circ}$ the perpendicular speed at re-encounter is always greater than at the initial encounter. Thus, in this geometry the returning ion should penetrate the shock into the downstream region. This is not, however, sufficient to insure that the ion will end up downstream. Simulations and a recent calculation of test particle

trajectories show that for $45^{\circ} < \theta_{Bn} \lesssim 60^{\circ}$, there are trajectories which allow a reflected ion to gyrate back upstream after initial penetration of the shock surface (Leroy and Winske, 1983; Burgess and Schwartz, 1984).

Measurements made both up and downstream from the earth's bow shock are in accord with the predictions of the above calculations. For example, Sckopke et al. (1983) have noted that nearly specularly reflected ions play an important role in producing downstream ion thermalization at supercritical shocks for all $\theta_{Bn} \gtrsim 45^{\circ}$. Further, ions gyrating upstream away from the shock and having guiding center velocities and gyrospeeds consistent with specular reflection have been observed in the quasi-parallel geometry. Figure 10 shows examples of gyrating ion velocity distributions observed upstream from a crossing of the quasi-parallel shock ($\theta_{Bn} = 37^{\circ}$). As in Figures 4 and 5 the velocity distributions are presented as contours of equal phase space density, f, in 2-dimensional velocity space oriented parallel to the ecliptic. The vectors drawn through the incident solar wind distributions represent the ecliptic projections of the extreme orientation of $\underline{B}$ measured during the 3 s plasma measurement interval. The bars drawn perpendicular to $\underline{B}$ in each panel provide a direct comparison with the specular reflection model. The positions of the centers of these bars are the predicted guiding center velocities of the reflected ions, and their half-lengths are the predicted gyrospeeds. These calculated motions of the secondary ions are in reasonably good agreement with the observations.

We have previously emphasized the very important role nearly specularly reflected ions play in producing downstream ion thermalization at supercritical shocks when $\theta_{Bn} \gtrsim 45^{\circ}$. On the other hand, when $\theta_{Bn} \lesssim 45^{\circ}$ nearly specularly reflected ions gyrate back upstream when the field is steady and thus cannot contribute directly to downstream thermalization under such conditions. How,

then, is downstream ion thermalization produced at supercritical shocks in the quasi-parallel geometry? One possibility is that dissipation in the quasi-parallel geometry occurs by means other than or in addition to ion reflection (e.g., Quest et al., 1983). Another possibility is that waves generated by the backstreaming, reflected ions produce a slowly variable $\theta_{Bn}$ at the shock such that reflected ions are alternately directed up or downstream depending upon the instantaneous value of $\theta_{Bn}$ (Gosling et al., 1984). In support of this suggestion we note that: a) long period upstream waves appear to be an intrinsic feature of the quasi-parallel shock (e.g., Greenstadt and Fredricks, 1979); and b) all of the specularly reflected ion events in the quasi-parallel geometry studied to date are found in close association with such waves (Thomsen et al., 1984). Whether or not the above suggestion has any merit, it is clear that further studies of the ion reflection phenomenon in the quasi-parallel geometry should lead to a better understanding of the supercritical, quasi-parallel shock.

## Summary

To summarize this brief review we wish to emphasize the following points:

1. Ion reflection is the dominant ion dissipation mechanism at nearly perpendicular, supercritical shocks.
2. An increasing fraction of the ions incident on a supercritical shock is reflected as the Mach number increases. The actual fraction reflected can be predicted using the Rankine-Hugoniot conservation relations.
3. The effective temperature associated with the dispersion in velocity space associated with ion reflection accounts for a large fraction of the temperature rise observed across supercritical, quasi-perpendicular shocks.

4. Solar wind ions are essentially unmagnetized for single encounters with the Earth's bow shock. As a result, ion reflection at the shock is nearly specular.
5. The subsequent trajectory of an ion nearly specularly reflected at the shock is controlled by $\theta_{Bn}$.
6. For $\theta_{Bn} > 45^{o}$, the guiding center motions of a specularly reflected ion is directed downstream. Reflected ions returning to the shock in this geometry should be able to penetrate through the shock.
7. In the above geometry, the downstream ion f(v) consists initially of a directly transmitted, slightly heated core population plus a population of phase-bunched, gyrating ions moving on a circle of radius $2\ V_i\ \cos\theta_{vn}$.
8. For $\theta_{Bn} < 45^{o}$, the guiding center motion of a nearly specularly reflected ion is directed back upstream. When the upstream field is steady, such ions cannot contribute directly to downstream ion thermalization.

Acknowledgement

J. Gosling has collaborated closely with W. C. Feldman, G. Paschmann, S. J. Schwartz, N. Sckopke, and M. F. Thomsen on many of the topics discussed in this review. He has benefited greatly from their collective wisdom. The work at Los Alamos was performed under the auspices of the Department of Energy and was supported in part by NASA through the ISEE program (contract number S-50864A). Work at NRL ....

## References

Asbridge, J. R., S. J. Bame, J. T. Gosling, G. Paschmann, and N. Sckopke, Energetic plasma ions within the earth's magnetosheath, Geophys. Res. Lett., 5, 953-955, 1978.

Bame, S. J., J. R. Asbridge, H. E. Felthauser, J. P. Glore, G. Paschmann, P. Hemmerich, K. Lehmann, and H. Rosenbauer, ISEE-1 and ISEE-2 fast plasma experiment and the ISEE-1 solar wind experiment, IEEE Transact. Geosci. Electron., GE-16, 216, 1978.

Bame, S. J., J. R. Asbridge, H. E. Felthauser, J. P. Glore, G. Paschmann, P. Hemmerich, K. Lehmann, and H. Rosenbauer, High temporal resolution observations of electron heating at the bow shock, Space Sci. Rev., 23, 75, 1979.

Burgess, D., and S. J. Schwartz, The dynamics and upstream distributions of ions reflected at the earth's bow shock, J. Geophys. Res., in press, 1984.

Coronitti, F. V., Dissipation discontinuities in hydromagnetic shock waves, J. Plasma Phys., 4, 265, 1970.

Feldman, W. C., J. R. Asbridge, S. J. Bame, and J. T. Gosling, Plasma and magnetic fields from the Sun, in: The Solar Output and Its Variation (O. R. White, ed.), pp. 351-382, Boulder, CO (Colorado Associated Univ. Press), 197/.

Formisano, V., and P. C. Hedgecock, On the structure of the turbulent bow shock, J. Geophys. Res., 78, 6522, 1973.

Goodrich, C. C., Numerical Simulations of Collisionless Shocks, this volume.

Gosling, J. T., J. R. Asbridge, S. J. Bame, A. J. Hundhausen, and I. B. Strong, Satellite observations of interplanetary shock waves, J. Geophys. Res., 73, 43, 1968.

Gosling, J. T., M. F. Thomsen, S. J. Bame, W. C. Feldman, G. Paschmann, and N. Sckopke, Evidence for specularly reflected ions upstream from the quasi-parallel bow shock, Geophys. Res. Lett., 9, 1333, 1982.

Gosling, J. T., M. F. Thomsen, S. J. Bame, and M. Mellott, Ion and electron heating at the quasi-parallel bow shock, paper presented at Chapman Conference on Collisionless Shocks in the Heliosphere, Napa, CA, February 1984.

Greenstadt, E. W., and R. W. Fredricks, Shock systems in collisionless space plasmas, in Solar System Plasma Physics, Vol. III, edited by L. J. Lanzerotti, C. F. Kennell, and E. N. Parker, p3, North-Holland, Amsterdam, 1979.

Gurgiolo, C., G. K. Parks, and B. H. Mauk, Upstream gyrophase bunched ions: a mechanism for creation at the bow shock and the growth of velocity space structure through gyrophase mixing, J. Geophys. Res., 88, 9093, 1983.

Holzer, R. E., M. G. McLeon, and E. J. Smith, Preliminary results from the Ogo 1 search coil magnetometer: boundary positions and magnetic noise spectra, J. Geophys. Res., 71, 1481, 1966.

Leroy, M. M., and D. Winske, Backstreaming ions from oblique Earth bow shocks, Ann. Geophys., 1, 527, 1983.

Leroy, M. M., C. C. Goodrich, D. Winske, C. S. Wu, and K. Papadopoulos, Simulation of a perpendicular bow shock, Geophys. Res. Lett., 8, 1269, 1981.

Leroy, M. M., D. Winske, C. C. Goodrich, C. S. Wu, and K. Papadopoulos, The structure of perpendicular bow shocks, J. Geophys. Res., 87, 5081, 1982.

Livesey, W. A., C. F. Kennel, and C. T. Russell, ISEE-1 and -2 observations of magnetic field strength overshoots in quasi-perpendicular bow shocks, Geophys. Res. Lett., 9, 1037, 1982.

Mellott, M., and E. W. Greenstadt, The structure of oblique subcritical bow shocks: ISEE 1 and 2 observations, J. Geophys. Res., 89, 2151, 1984.

Montgomery, M. D., J. R. Asbridge, and S. J. Bame, Vela 4 plasma observations near the earth's bow shock, J. Geophys. Res., 75, 1217, 1970.

Ness, N. F., C. S. Searce, and J. B. Seek, Initial results on the IMP 1 magnetic field experiment, J. Geophys. Res., 69, 3531, 1964.

Neugebauer, M., Initial deceleration of solar wind positive ions in the Earth's bow shock, J. Geophys. Res., 75, 717, 1970.

Paschmann, G., and N. Sckopke, Ion reflection and heating at the earth's bow shock, in Topics in Plasma-, Astro-, and Space Physics, p. 139, edited by G. Haerendel and B. Battrick, MPI für Physik und Astrophysik, 8046 Garching, W. Germany.

Paschmann, G., N. Sckopke, S. J. Bame, and J. T. Gosling, Observations of gyrating ions in the foot of the nearly perpendicular bow shock, Geophys. Res. Lett., 9, 881, 1982.

Paul, J. W. M., Review of experimental studies of collisionless shocks propagating perpendicular to a magnetic field, in Collision-Free Shocks in the Laboratory and Space, ESRO SP-51, p. 97, 1969.

Paul, J. W. M., L. S. Holmes,M. J. Parkinson, and J. Sheffield, Experimental observations on the structure of collisionless shock waves in a magnetized plasma, Nature, 208, 133, 1965.

Phillips, P. E., A study of the structure of collisionless shock waves propagating perpendicular to an initial field, Thesis, Physics Department, The University of Texas, December 1971.

Phillips, P. E., and A. E. Robson, Influence of reflected ions on the magnetic structure of a collisionless shock front, Phys. Rev. Lett., 29, 154, 1972.

Quest, K. B., D. W. Forslund, J. U. Brackbill, and K. Lee, Collisionless dissipation processes in quasi-parallel shocks, Geophys. Res. Lett., 10, 471, 1983.

Robson A. E., Experiments on oblique shock waves, in Collision-Free Shocks in the Laboratory and Space, ESRO SP-51, p. 159, 1969.

Russell, C. T., and E. W. Greenstadt, Initial ISEE magnetometer results: Shock observations, Space Sci. Rev., 23, 3, 1979.

Sanderson, J. J., and R. A. Uhrig, Extended Rankine-Hugoniot relations for collisionless shocks, J. Geophys. Res., 83, 1395, 1978.

Schwartz, S. J., M. F. Thomsen, and J. T. Gosling, Ions upstream of the earth's bow shock: a theoretical comparison of alternative source populations, J. Geophys. Res., 2039, 1983.

Sckopke, N., G. Paschmann, S. J. Bame, J. T. Gosling, and C. T. Russell, Evolution of ion distributions across the nearly perpendicular bow shock: specularly and non-specularly reflected-gyrating ions, J. Geophys. Res., 88, 6121, 1983.

Sonett, C. P., D. S. Colburn, L. Davis, E. J. Smith, and P. J. Coleman, Evidence for a collision-free magnetohydrodynamic shock in interplanetary space, Phys. Rev. Lett, 13, 153, 1964.

Thomsen, M. F., Suprathermal ions upstream of the earth's bow shock, this volume, 1984.

Thomsen, M. F., S. J. Schwartz, and J. T. Gosling, Observational evidence on the origin of ions upstream of the earth's bow shock, J. Geophys. Res., 88, 7843, 1983.

Thomsen, M. F., J. T. Gosling, S. J. Bame, and C. T. Russell, Gyrating ions and large-amplitude, monochromatic MHD waves upstream of the earth's bow shock, J. Geophys. Res., submitted, 1984.

Winske, D., Microtheory of collisionless shock current layers, this volume, 1984.

Woods, L. C., On the structure of collisionless magneto-plasma shock waves at supercritical Alfvén-Mach numbe[illegible] Plasma Phys., 3, 435, 1969.

## Figure Captions

Figure 1. Magnetic field and electric potential profiles of a subcritical shock (upper panel) and a supercritical shock (lower panel) for $\theta_{Bn} = 90^{\circ}$ (from Paul et al., 1965). For $M_A \gtrsim 3$, a foot of length 0.7 Rgi develops upstream of the main shock ramp. Here Rgi is an ion gyroradius for a particle with speed equal to the shock speed through the ambient plasma. A small overshoot in the potential occurs at the back of the shock ramp in the supercritical regime. Similar overshoots in $\underline{B}$ and electron pressure are commonly observed at the Earth's bow shock (e.g., Livesey et al., 1982; Bame et al., 1979).

Figure 2.a. Idealized sketch of the trajectory of an ion specularly reflected off a planar shock with $\theta_{Bn} = 90^{\circ}$ for arbitrary angle of incidence.

b. Idealized 2-dimensional ion velocity distributions resulting from specular reflection at several distances from the shock ramp. The reflected particles move in velocity space along a circle of radius $2\,V\cos\theta_{vn}$ centered at the bulk flow velocity. The dashed lines indicate the orientation of the shock surface.

Figure 3. Electric potential jump at the shock (upper panel) and reflected ion current (lower panel) as functions of $M_A$ for $\theta_{Bn} = 90^\circ$. The potential jump is normalized to the incident ion flow energy (from Phillips, 1971).

Figure 4. Ion velocity distributions obtained during an inward crossing of the Earth's bow shock. Each panel represents a 3 sec snapshot of f(v) obtained at the locations indicated by the dots on the electron density profiles shown as inserts. The distributions are shown as contours of constant phase space density separated logarithmically in 2-dimensional velocity space, where one of the axes points toward the sun on the left, and the + symbol indicates zero speed in the spacecraft frame. The dashed lines indicate the orientation of the shock surface (from Paschmann and Sckopke, 1983).

Figure 5. Ion velocity distributions obtained downstream of a marginally supercritical shock with $\theta_{Bn} \approx 90^\circ$ and $\underline{B}$ oriented nearly perpendicular to the measurement plane of the instrument. The format is similar to Figure 4 except that more contour levels are shown. The dashed circle in the second frame indicates the expected locus of specularly reflected ions in the downstream region (from Sckopke et al., 1983).

Figure 6. Time sequence of 1-dimensional ion distributions downstream of the shock crossing shown in Figure 4. The cuts were made in the direction of the bulk flow. Units for energy are in keV, and f is in units of $cm^6\ s^{-3}$ (from Sckopke et al., 1983).

Figure 7. Theoretically predicted ion reflectivity of the bow shock as a function of magnetosonic Mach number. The two curves refer to different upstream temperatures corresponding to $\beta_i = 0.1$ and 10, respectively. The filled-in symbols are spacecraft measured values, and the asterisks

indicate values obtained from numerical simulation studies (from Paschmann and Sckopke, 1983).

Figure 8. A series of planar vector diagrams illustrating the guiding center velocity, $\underline{V}_{gc}$, and gyrational motion $|\underline{V}_g|$ resulting from specular reflection of an ion initially incident on a supercritical shock with the plasma bulk flow velocity, $\underline{V}_1$, in different $\theta_{Bn}$ geometries. The initial reflected velocity, $\underline{V}_r$, is obtained by reversing the normal component of $\underline{V}_1$. Note that the reflected ion must have the same $\underline{E} \times \underline{B}$ drift, $\underline{V}_1$, as the incident plasma flow.

Figure 9. Gyrophase angle ($\Omega t^*$) and normal velocity ($v_n(t^*)$), in units of the normal component of the incident flow velocity, $\underline{v}_1$) of a specularly reflected ion at the time of re-encounter with the shock, $t^*$, as a function of $\theta_{Bn}$ (from Schwartz et al., 1983).

Figure 10. Ion velocity distributions obtained upstream from the bow shock for $\theta_{Bn} \approx 37^\circ$ and $\underline{B}$ nearly in the measurement plane of the instrument. The format is similar to Figures 4 and 5. Tic marks and numbers in the lower right of each panel indicate the velocity scale in km $s^{-1}$. The extreme orientations of the magnetic field vector within each 3 s measurement interval are indicated by the vectors $\underline{B}_1$, $\underline{B}_2$ drawn through the center of the incident solar wind. The ends of the bars drawn perpendicular to $\underline{B}$ indicate the expected positions in velocity space of specularly reflected ions (from Gosling et al., 1982).

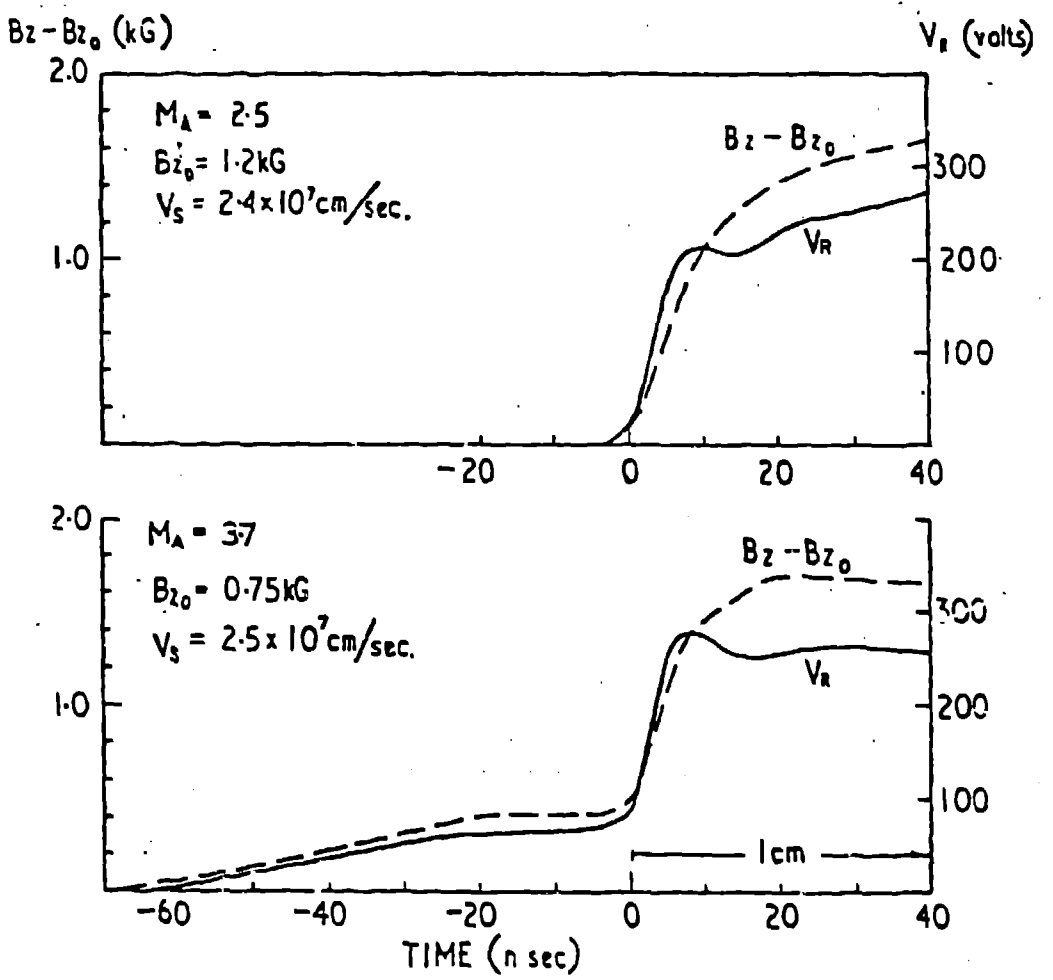
Bz - Bz₀ (kG)
V_R (volts)
2.0
1.0
M_A = 2·5
Bz₀ = 1·2kG
V_S = 2·4 x 10⁷ cm/sec.
Bz - Bz₀
V_R
300
200
100
-20
0
20
40
2·0
1·0
M_A = 3·7
Bz₀ = 0·75kG
V_S = 2·5 x 10⁷ cm/sec.
Bz - Bz₀
V_R
300
200
100
1cm
-60
-40
-20
0
20
40
TIME (n sec)

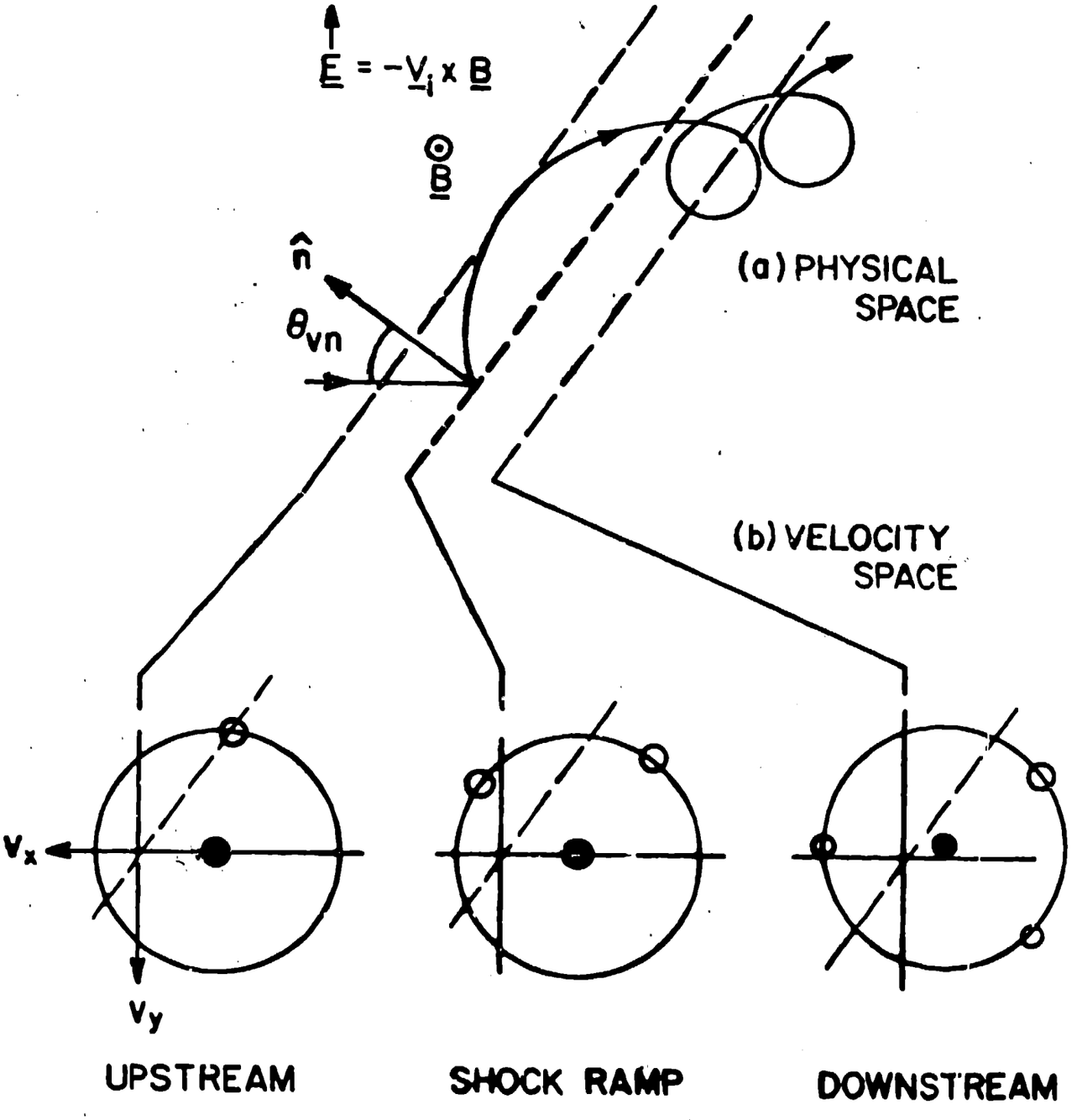
$\underline{E} = -\underline{V}_i \times \underline{B}$
$\underline{B}$
$\hat{n}$
$\theta_{vn}$
(a) PHYSICAL SPACE
(b) VELOCITY SPACE
$V_x$
$V_y$
UPSTREAM
SHOCK RAMP
DOWNSTREAM

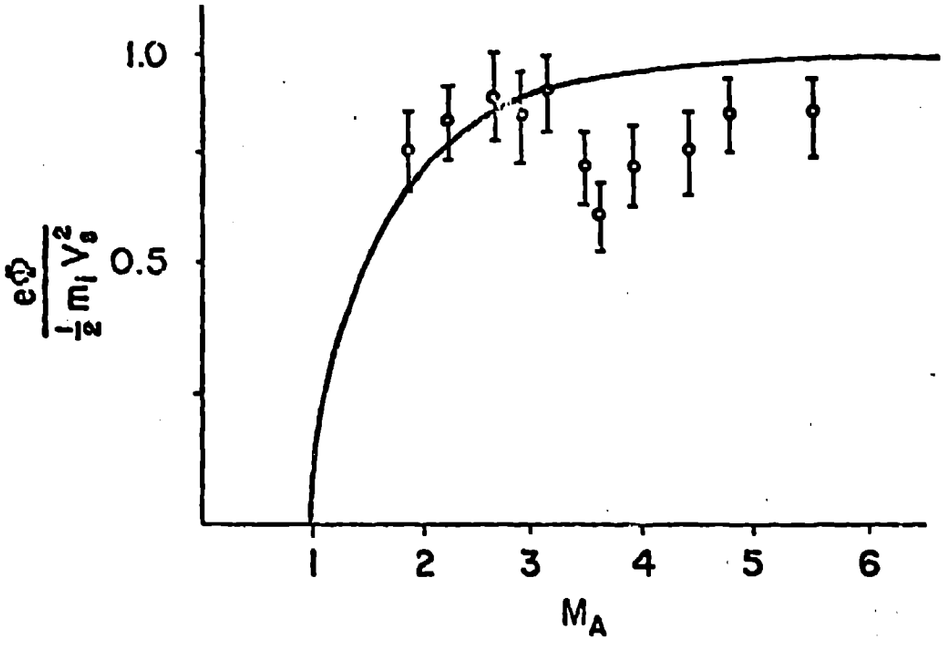
1.0
0.5
$\frac{e\Phi}{\frac{1}{2}m_i V_0^2}$
1
2
3
4
5
6
$M_A$

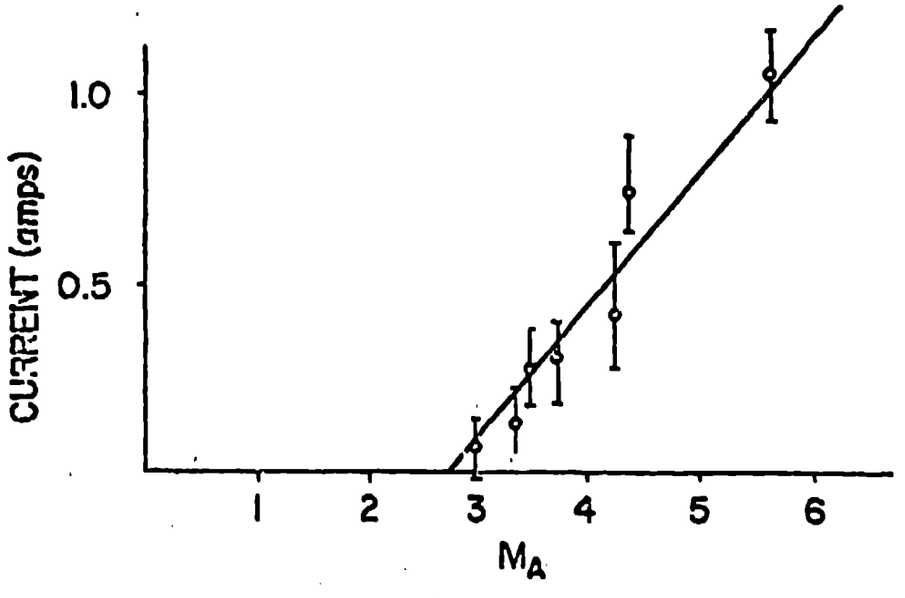
1.0
0.5
CURRENT (amps)
1
2
3
4
5
6
$M_A$

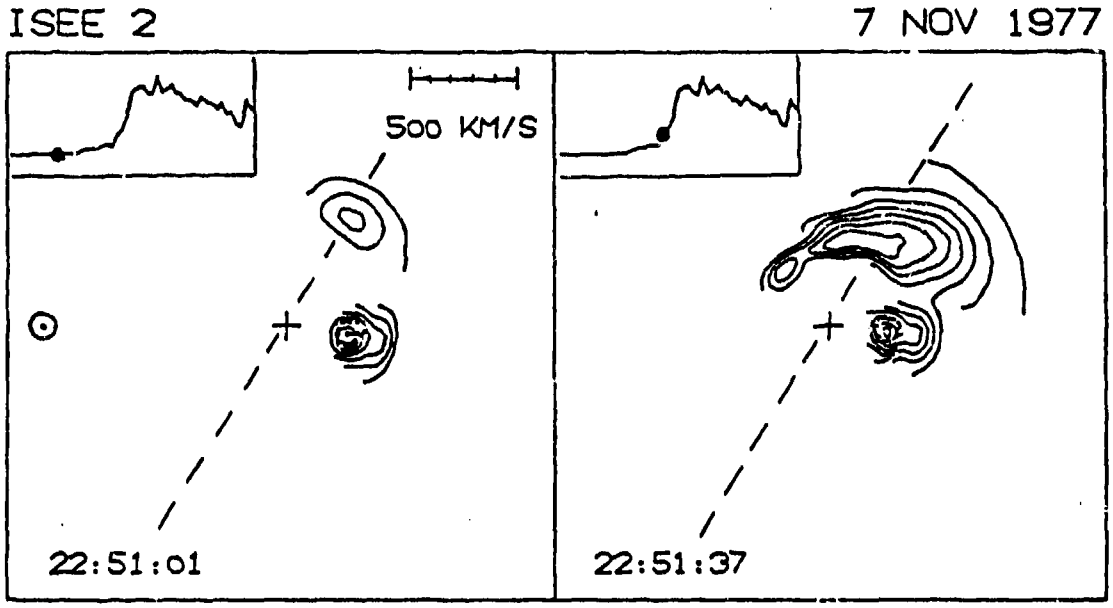
ISEE 2
7 NOV 1977
500 KM/S
22:51:01
22:51:37

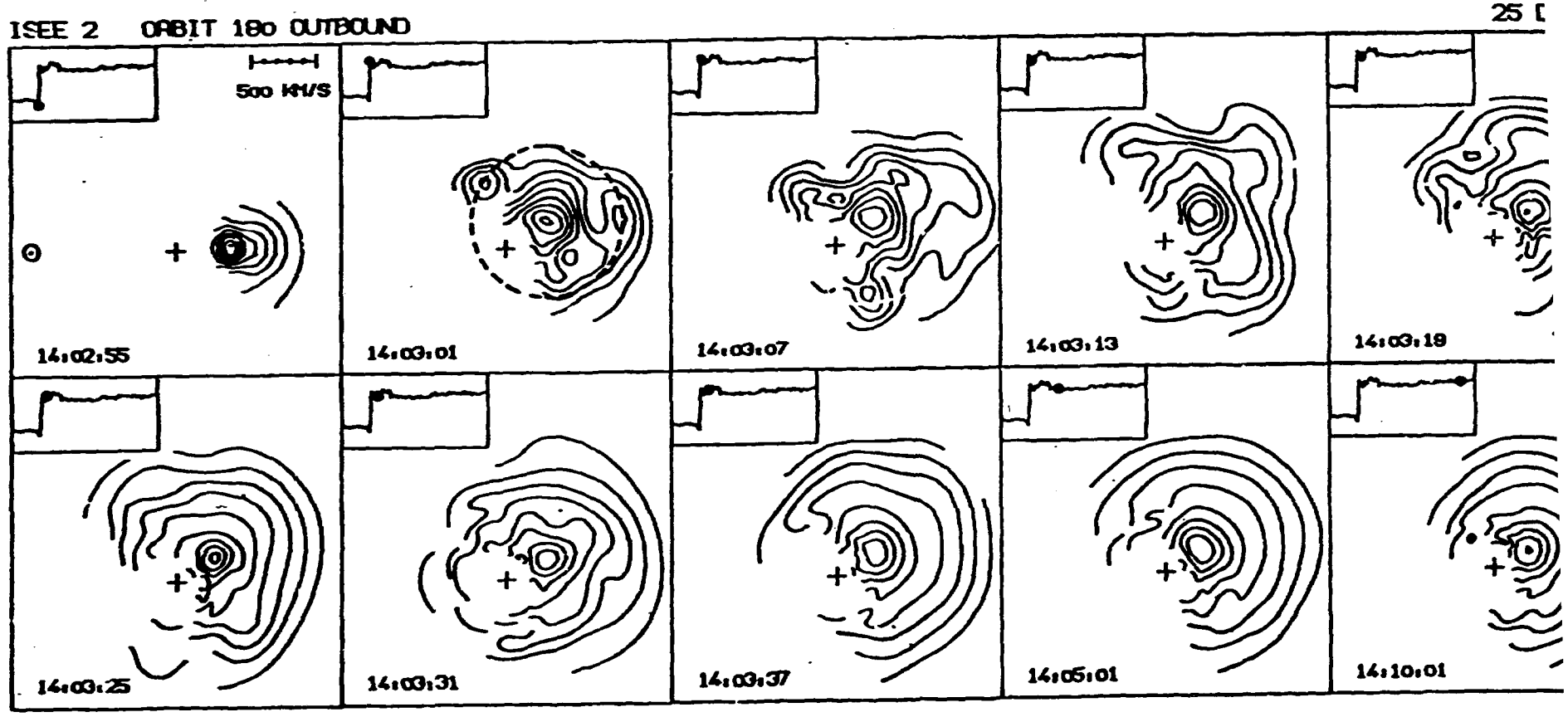
ISEE 2 ORBIT 180 OUTBOUND
500 KM/S
14:02:55
14:03:01
14:03:07
14:03:13
14:03:19
14:03:25
14:03:31
14:03:37
14:05:01
14:10:01

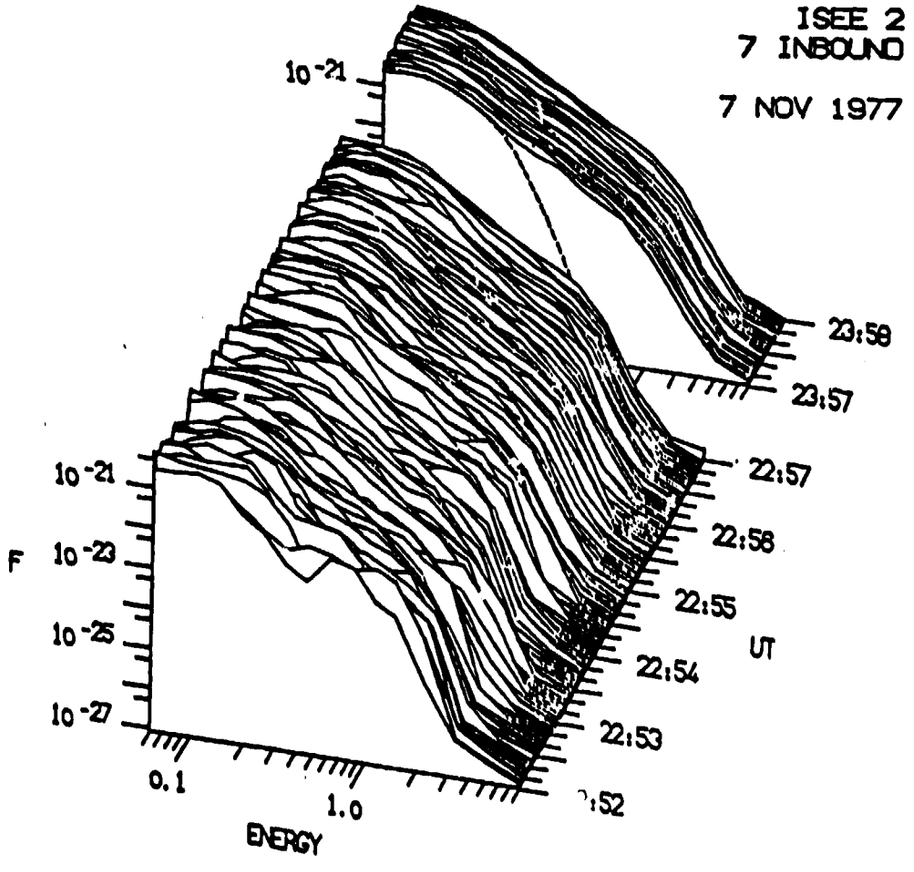
ISEE 2
7 INBOUND
7 NOV 1977
10-21
23:58
23:57
22:57
22:58
22:55
22:54
22:53
22:52
UT
10-21
10-23
10-25
10-27
F
0.1
1.0
ENERGY

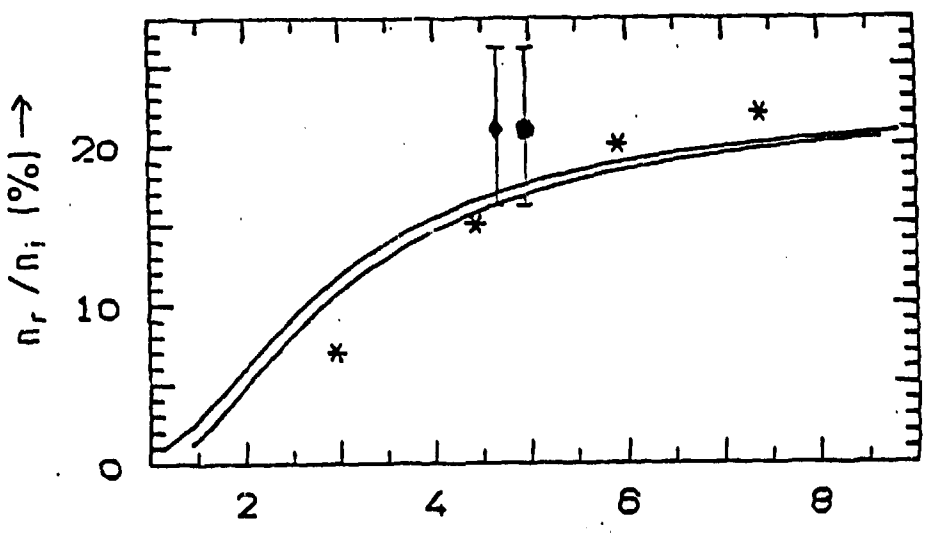
$n_r / n_i$ (%) →
0
10
20
2
4
6
8
$M_{ms}$ →

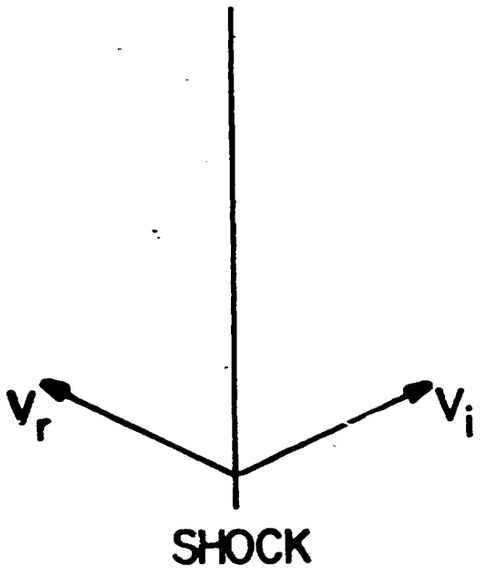
$V_r$
$V_i$
SHOCK

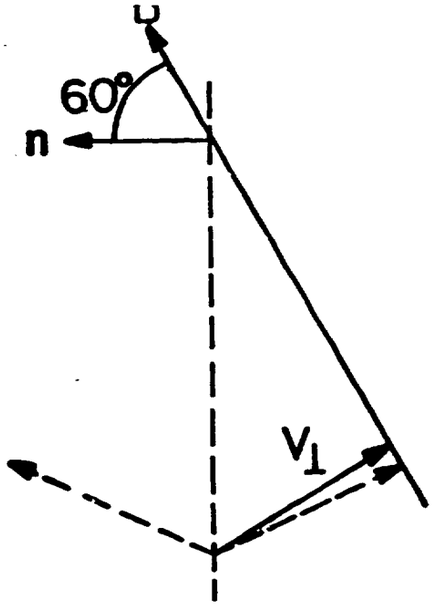
60°
n
$V_\perp$

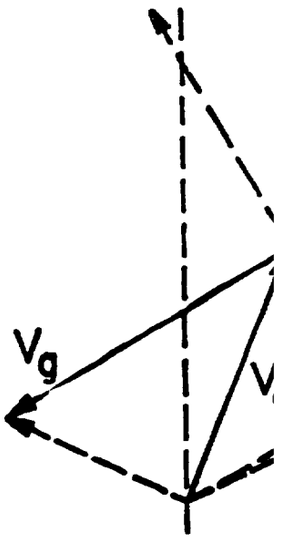
$V_g$

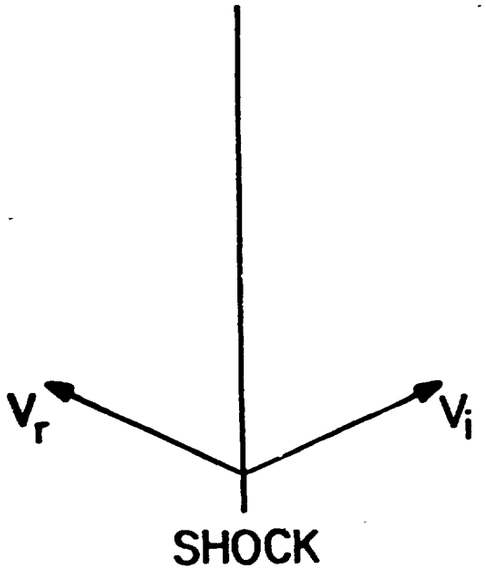
$V_r$
$V_i$
SHOCK

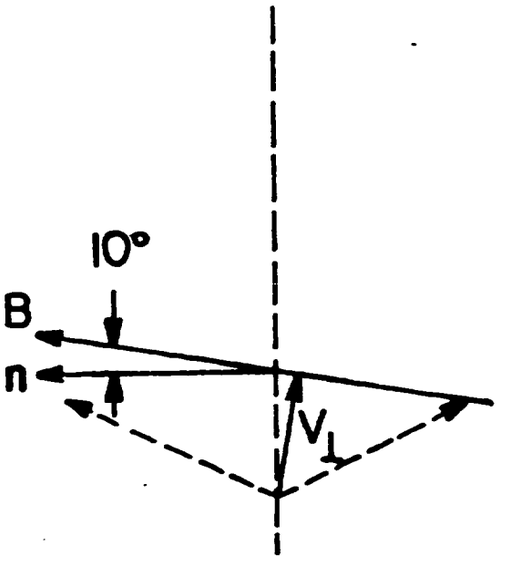
10°
B
n
$V_\perp$

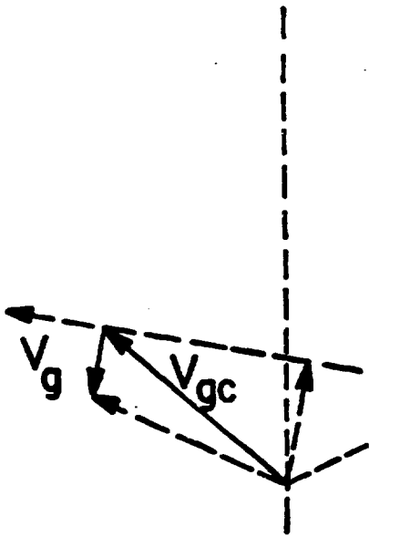
$V_g$
$V_{gc}$

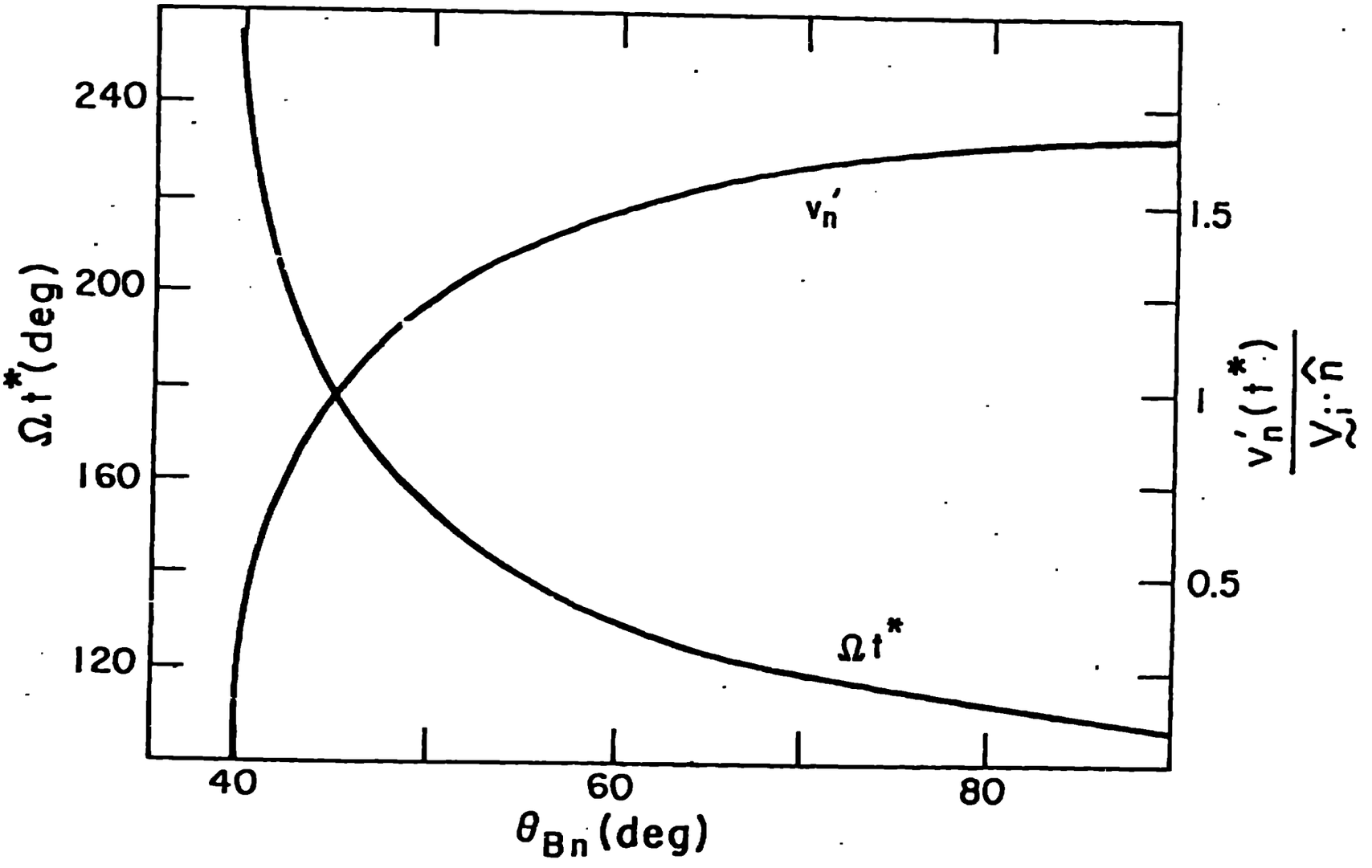


(5)

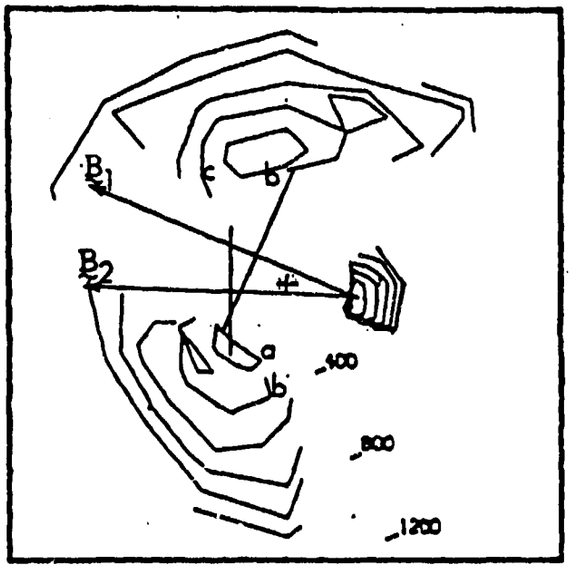


1222:59.8 - 1223:02.4 UT

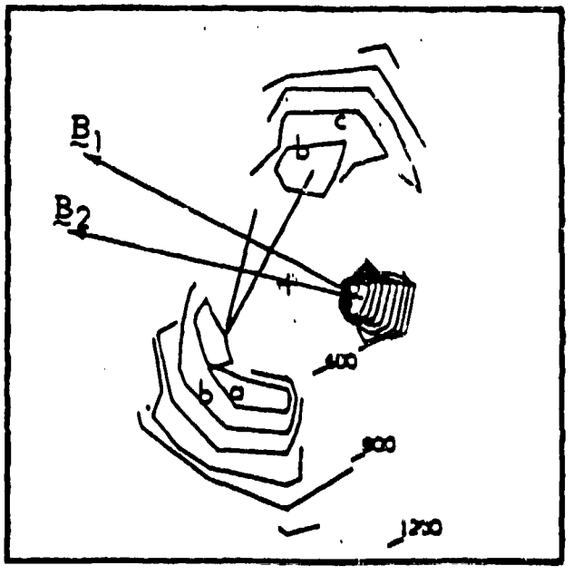


1223:35.8 - 38.4 UT